Superconducting phase diagram and the evolution of electronic structure across charge density wave in underdoped $1T$-Cu$_\delta$TiSe$_2$ under hydrostatic pressure

Shuxiang Xu,[1,2] Pengtao Yang ●,[1] Keyu Chen ●,[1] Ziyi Liu,[1] Wuwei Cui,[1] Qing Hu,[3] Jianping Sun ●,[1,2] Ran Ang ●,[3,5,*]
Yoshiya Uwatoko,[4] Bosen Wang,[1,2,6,*] and Jinguang Cheng ●[1,2,*]

[1]*Beijing National Laboratory for Condensed Matter Physics and Institute of Physics, Chinese Academy of Sciences, Beijing 100190, China*
[2]*School of Physical Sciences, University of Chinese Academy of Sciences, Beijing 100190, China*
[3]*Key Laboratory of Radiation Physics and Technology, Ministry of Education, Institute of Nuclear Science and Technology,*
Sichuan University, Chengdu 610064, China
[4]*Institute for Solid State Physics, University of Tokyo, Kashiwanoha 5-1-5, Kashiwa, Chiba 277-8581, Japan*
[5]*Institute of New Energy and Low-Carbon Technology, Sichuan University, Chengdu 610065, China*
[6]*Songshan Lake Materials Laboratory, Dongguan, Guangdong 523808, China*

We revisit a superconducting phase diagram and electronic structures across the charge density wave (CDW) phase transition of Cu-underdoped $1T$-Cu$_\delta$TiSe$_2$ ($\delta \sim 0.03$) under hydrostatic pressure. Superconductivity appears right after the complete collapse of the long-range CDW at a critical pressure of $P_c \sim 2.48$ GPa, apart from the reported superconducting phase diagrams; it is found that the superconducting transition temperature shows a domelike pressure dependence covering a narrow pressure range with a maximum of $T_c^{max} \sim 2.80$ K at 4.80 GPa. Accordingly, the residual resistivity ρ_0 and temperature exponent n of normal-state resistivity (from ~ 3.30 at ambient pressure to ~ 2.38 at P_c and ~ 4.0 at 6.50 GPa) reduce sizably while the quadratic temperature coefficient A of normal-state resistivity is enhanced by one order in magnitude; these results indicate the importance of CDW quantum fluctuation in superconducting pairing; low-T resistivity upwarps with a $-\ln T$ dependence below a characteristic temperature T^* which has a domelike shape in the pressure range of 2.82–4.80 GPa. Based on two-band analysis of Hall conductivity and Kohler-fitting of magnetotransport (MR), energy bands are dominated by electron-type carriers across the CDW phase transition for $P < P_c$, and they reverse into hole-type for $P > P_c$; interestingly, the mobility of carriers increases up to five times at P_c, but carrier concentration shows a weak pressure dependence. The MR value increases with the pressure for $P < P_c$ and then jump up to a saturated value after the collapse of the CDW. Our results show that the collapse of the CDW is accompanied by the reconstruction of the Fermi surface, and the enhancement in MR can be mainly attributed to the change of mobility. Possible mechanisms are discussed.

I. INTRODUCTION

$1T$-TiSe$_2$ is a typical transition-metal dichalcogenide (TMD), and has been studied extensively for many years [1–4]. In particular, its strong electronic interaction and electron-phonon coupling make it a classic candidate to study the interplay of charge density wave (CDW) and superconductivity (SC) as well as the underlying physical mechanisms [2,5–7]. But several topics remain controversial, especially for phase diagrams since the discovery of SC [3,5,8,9]. Thus, more studies on electronic structures can reveal new physics.

$1T$-TiSe$_2$ is a semimetal or small-gap semiconductor in its normal state, developing a commensurate CDW with a $2a_0 \times 2a_0 \times 2c_0$ superlattice structure at temperatures below ~ 200 K [10]. SC of $1T$-TiSe$_2$ was first discovered by the Cu ion intercalation into the Ti-Se interlayer through the suppression of the CDW [3,4]; SC of $1T$-Cu$_x$TiSe$_2$ occurs at $x = 0.04$, and the superconducting transition temperature

shows a domelike shape as a function of Cu composition with a maximum ~ 4.15 K at $x = 0.08$ [3]; such phase diagrams resemble those of unconventional high-T_c superconductors and heavy-fermion materials where strong competition and cooperation of low-energy excited states is thought to be one of the important glues for superconducting pairings [11,12]. Similar phase diagrams are also achieved in $1T$-TiSe$_2$ by the ion-gated technology, element intercalation, chemical doping, and physical pressure [3–5,13]. As reported previously, $1T$-TiSe$_2$ enters into a superconducting state with the suppression of the CDW by a pressure of 2–4 GPa [5], but the maximum of $T_c^{onset} \sim 1.80$ K is much lower than that of $1T$-Cu$_x$TiSe$_2$ [4,5]; meanwhile, unconventional pairing mechanisms of SC were also proposed in $1T$-TiSe$_2$ considering the indispensable hybridization of phonons and exciton modes [14]. For these phase diagrams, one common feature is the overlaps of CDW and SC in the underdoped area, which is the direct evidence of strong interplay between CDW and SC [3–5,13]. More studies make clear that the enhancement of CDW fluctuation seems to be important for superconducting pairing since CDWs and SC are both correlated intimately with the enhancement of electron-phonon coupling and Fermi

---

*Corresponding authors: rang@scu.edu.cn, bswang@iphy.ac.cn, and jgcheng@iphy.ac.cn

surface instabilities [2,5,13]. In addition to the macroscopic electrical transports x-ray technology was adopted to detect the detailed evolution of CDW order after the collapse of the long-range CDW [8,9]. It was found that the short-range CDW exists just above domelike T_c in $1T$-Cu$_{1-x}$TiSe$_2$, which implies close connections of superconducting pairings and CDW fluctuations [9]. However, contrary to the above viewpoints, several experimental investigations do not support the strong interplay between CDWs and SC [8]. As an example, the dome-shaped diagram was far from the long-range CDW in pure $1T$-TiSe$_2$, and weak connections between CDWs and SC were also concluded [8]. Another dispute involves the superconducting gap symmetry of Ti-Se materials: in one report, the superconducting state of $1T$-Cu$_{0.06}$TiSe$_2$ was argued to be a single-gap s-wave based on the specific heat results, and SC was not closely related to the suppression of the long-range CDW [15,16]; in another report, two superconducting gaps appear in $1T$-Cu$_x$TiSe$_2$, and a larger density of states emerges in the form of narrow electron pockets near the L point of the Brillouin zone. The d-like features of the bands and the order parameters compete microscopically with SC in the same energy level [17].

Electronic structures of $1T$-Cu$_x$TiSe$_2$ depend strongly on CDW states and the real Cu compositions [10,17,18]. $1T$-TiSe$_2$ undergoes the reconstruction of the Fermi surface across the CDW phase transition: electron-type carriers are dominated above T_{CDW}, while hole-type carriers exceed electron-type ones below T_{CDW} [6,7]. The differences provide distinct Fermi surface electron density and Fermi wave vectors across the CDW transition, and they result in large differences in electron-phonon couplings and superconducting properties [5,14]. In addition, the interplay of van der Waals coupling is another factor in electronic structures, and it also affects the interplay of CDW and SC [3,4,19,20]. The c axis elongates as the Cu-intercalation increases while shrinkings by pressure in $1T$-TiSe$_2$ [3–5,21]; as a result, the former bands are dominated by electron-type carriers, but more hole-type carriers are generated in the latter. At present, the application of physical pressure to adjust the lattice parameter and to study the evolution of the electronic structure of the Cu-underdoped $1T$-TiSe$_2$ should be quite valuable to understand superconducting phase diagrams and the common characteristic of the superconducting state. In this work, we revisit phase diagrams of CDW and SC as well as electronic structures of the Cu-underdoped $1T$-TiSe$_2$. A domelike SC emerges right after the complete collapse of the CDW; the dominant carriers are reversed from electron-type to hole-type across the CDW phase transition; the magnitude of mobility increases up to nearly five times at P_c. Our results suggest the reconstruction of the Fermi surface is associated with the pressure-induced collapse of the long-range CDW.

II. EXPERIMENTAL METHODS

Single-crystal $1T$-Cu$_\delta$TiSe$_2$ was grown by chemical vapor transport methods with the iodine as the transport agent, as reported elsewhere [3,4]. Single-crystal x-ray diffraction (XRD) and powder XRD confirm consistently that all the selected crystals $1T$-Cu$_\delta$TiSe$_2$ have good quality with a trigonal phase (space group: P-$3m1$, 164). According to the structural

refinement analysis of room-temperature powder XRD, lattice parameters are found to be about $a = b = 3.5420$ AA and $c = 6.0198$ Å, respectively, close to the reported values of $1T$-Cu$_\delta$TiSe$_2$ ($\delta \sim 0.035$) [3,4,21]; meanwhile, electrical resistivity and Hall resistivity were measured on the commercialized Quantum Design Physical Property Measurement System ($1.8 \leqslant T \leqslant 400$ K, $0 \leqslant H \leqslant 9$ T). It is found that the temperature dependence of resistivity shows a broad peak near a characteristic temperature ~ 150 K, which is much close to that of $1T$-Cu$_\delta$TiSe$_2$ ($\delta \sim 0.03$) according to previous studies of phase diagrams [3,4,21]. Our results confirm the high quality of single crystals in the Cu-underdoped level with $\delta \sim 0.03$.

A cubic anvil pressure cell (CAC) was used for measurements of magnetotransport and the Hall coefficient. It can generate hydrostatic pressures by triaxial compression and a liquid pressure transmitting medium (PTM) [22,23]. Pressure was determined by measuring phase transitions of single-crystal bismuth at 300 K and the superconducting phase transition of bulk lead at low temperature. Electrical resistivity was measured using the standard four-probe method with the current parallel to the ab plane of crystals and the field perpendicular to the c axis. For high-pressure measurements, the usual size of single crystals is about $0.60 \times 0.20 \times 0.20$ mm^3. Low-temperature experiments were performed on a homemade ^{4}He refrigerated cryostat ($1.4 \leqslant T \leqslant 295$ K and $0 \leqslant H \leqslant 9$ T).

III. RESULTS AND DISCUSSION

Figure 1 shows the temperature dependence of electrical transport $\rho(T)$ for $1T$-Cu$_\delta$TiSe$_2$ under various pressures up to 7.0 GPa. For S1# in run 1 and run 2, a broad peak is found in $\rho(T)$ at a characteristic temperature ~ 150 K at ambient pressure (AP) as shown in Figs. 1(a)–1(c). This value is close to the reported value of the $2a_0 \times 2a_0 \times 2c_0$ CDW phase transition in $1T$-Cu$_\delta$TiSe$_2$ ($\delta \sim 0.03$) according to previous studies [3,10,21]; the temperature dependence of the derivation $d\rho/dT$ was plotted in Figs. 1(d)–1(f) and its minimum peak is defined as the CDW phase transition T_{CDW}. With increasing pressure, T_{CDW} shifts down to lower temperatures, namely from ~ 150 K at AP to ~ 54.2 K at 2.0 GPa, and then cannot be found above 2.82 GPa; this indicates pressure-induced collapse of long-range CDW as reported in various TMD materials [20]; similar behaviors are also found for S2# in run3 as shown in Fig. S1, and the suppression of the CDW by pressure has no sample dependence [24]; for both, the critical pressure P_c for the complete collapse of the CDW will be discussed. Meanwhile, room-temperature resistivity decreases with quite different pressure slopes: its value reduces quickly for $P < P_c$ but slightly for $P > P_c$; especially, in a pressure range of 1.0–3.0 GPa, resistivity in the whole temperature range decreases jumpily to one-half, which can be attributed to the closure of the CDW energy gap and the increase of carrier concentration [3,5,20]. In the same way, CDW appears near ~ 159 K at AP for S2# in run3 as shown in Fig. S1 [24], consistent with that of S1#. Room-temperature resistivity at 7.0 GPa decreases to one-sixth of that at AP. Finally, these features consistently suggest the modification of electronic structures along with pressure-induced
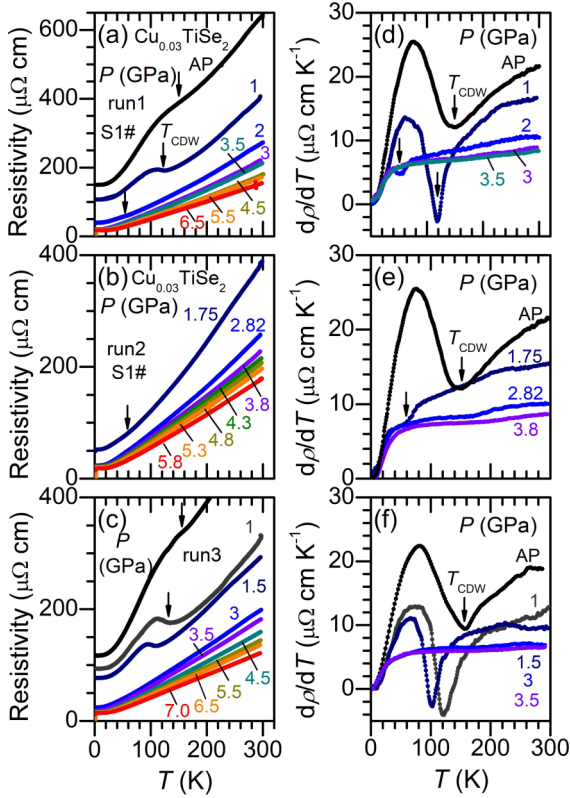
FIG. 1. $\rho(T)$ under pressures for $1T$-$Cu_{0.03}TiSe_2$ in different runs: (a) S1#, run1; (b) S1#, run2; and (c) S2#, run3. The derivatives $d\rho/dT$ are exported from $\rho(T)$ for (d) S1#, run1; (e) S1#, run2; and (f) S2#, run3, respectively. The black arrows indicate CDW transition and transition temperature T_{CDW} where $d\rho/dT$ reaches the minimum.

FIG. 2. Low-T $\rho(T)$ for (a) S1#, run1 and (b) S1#, run2; the arrows indicate the onset superconducting transition T_c^{onset} (blue) and zero resistivity temperature T_c^{zero} (black) where the resistivity starts to decrease and reaches zero. $\rho(T)$ and the fittings (solid lines), denoted by $\rho(T) = \rho_0 + AT^n$ with the residual resistivity ρ_0, the temperature coefficient A, and the exponent n, respectively: (c) 3.0–6.5 GPa, run1; (d) 3.0–7.0 GPa, run3. The insets of (c) and (d) show the enlargement of $\rho(T)$; the upturn temperature T^* in $\rho(T)$ is marked by red arrows; the blue arrows indicate T_c^{onset}. The pressure dependence of ρ_0 and n is summarized in Fig. 3.

collapse of the CDW through pressure-induced lattice distortions [7,20]. However, the short-range CDW may still exist, although there is no signal of CDW phase transition in resistivity [8,9,20,25]. Besides, weak resistivity hysteresis can be found as one feature of the first-order phase transition, apart from the electronic phase transition of pure $1T$-$TiSe_2$ around CDW phase transition according to the previous studies; one possible reason is the random distribution of small amounts of Cu intercalation and/or some possible atomic disorder concerning sample quality. The other reason is some atomic disorder which usually brings a symmetry-breaking charge domain structure, which introduces local conductance anisotropy and allows slow domain dynamics under pressures, which is responsible for the weak hysteresis effect.

Just after the collapse of the CDW, the superconducting transition starts to appear as reflected by a drop of low-T resistivity as plotted in Figs. 2(a) and 2(b); T_c^{onset} and T_c^{zero} are adopted to mark the onset superconducting phase transition and zero resistivity state, respectively. For S1# in run1 and run2, T_c^{onset} increases from ~ 1.50 K at 3.0 GPa to a maximum ~ 2.80 K at 4.80 GPa, and then decreases upon further increasing the pressure; no signature of SC is found down to 1.40 K above 6.50 GPa. T_c^{zero} is achieved covering a narrow pressure range, from ~ 1.67 K at 4.30 GPa to a maximum of ~ 2.10 K at 4.80 GPa, and it reduces to ~ 2.05 K at 5.30 GPa.

A similar pressure dependence of T_c^{onset} and T_c^{zero} was found in S2#, and the data are shown in Fig. 3(a). Such a narrow pressure range of T_c^{zero} indicates that the binding energy of the Cooper pair should be smaller and sensitive to the external physical pressure [5,17].

Interestingly, some unusual features of low-T normal-state resistivity appear just after the collapse of the CDW at P_c as in Figs. 2(c)–2(d). Low-T resistivity upwarps below a characteristic temperature T^* as shown in the inset of Figs. 2(c)–2(d). We find that this upturn of resistivity does not depend on samples and is intrinsic for crystals; for each crystal, low-T resistivity shows a $-\ln T$-temperature dependence below a characteristic temperature T^*, which is the common feature of Kondo-like scatterings [26]. The T^* value changes sensitively as a function of pressure and shows a domelike pressure dependence in the range of 2.82–4.80 GPa. T^* is just above T_c^{onset} of SC, T^* is 4.7 K at 2.82 GPa, and it enhances up to 9.38 K around 3.50–3.80 GPa and then reduces to zero above 4.80 GPa, where T_c^{onset} and T_c^{zero} reach the maximal value. The close relationships of T^* and T_c^{onset} and/or T_c^{zero} strongly suggest that there should be some other excess scatterings competing with the superconducting state [5,20]. Usually, Kondo-like scatterings come from the correlations between local magnetic spins and free electrons in metals with magnetic impurities [26]. However, according to Refs. [5,7,13,20], CDW materials behave as an ordinary metal
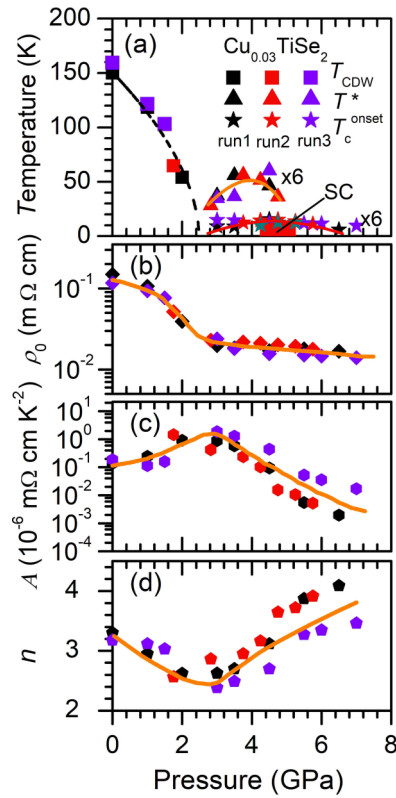
FIG. 3. (a) Temperature-pressure phase diagram of $1T$-$Cu_{0.03}TiSe_2$. T_{CDW}, T^*, and T_c^{onset} represents the CDW transition temperature, the upturn temperature in resistivity, and the superconducting transition temperature, respectively. The square points represent T_{CDW} and the black solid line is the fittings by $T_{CDW}(P) = T_0(1-P/P_c)^\beta$; where T_0, P_c, and β represent T_{CDW} at AP, the critical pressure where T_{CDW} reduces to zero, and the pressure exponent characterizing the suppression of CDW, respectively. The fittings of normal-state resistivity by $\rho(T) = \rho_0 + AT^n$ give (b) ρ_0, (c) A, and (d) n. A is linearly fitted with $n = 2$. The solid lines show the changing trends.

and/or contain some short-range CDW after the collapse of long-range CDW [9,25]. However, in these crystals, there are no more magnetic scatterings applied to free electrons. Thus, the origin of Kondo-like behavior requires clarification, and random distributions of the Cu ion between Ti-Se interlayer may block electron transport.

A temperature-pressure phase diagram is plotted in Fig. 3(a). It is found that T_{CDW} of $1T$-$Cu_{0.03}TiSe_2$ decreases rapidly with increasing pressure and disappears above a critical pressure P_c. According to Refs. [8,20], the pressure dependence of T_{CDW} can be well-fitted by the empirical formula $T_{CDW} = T_0(1-P/P_c)^\beta$, where T_0, P_c, and β represent T_{CDW} at AP, the critical pressure where T_{CDW} reduces to zero, and the exponent, respectively [8,20,27,28]. The fittings gave the parameters $T_0 \sim 150.54$ K, $P_c \sim 2.482$ GPa, and $\beta \sim 0.551$, respectively. We note that the β is close to the reported values from different techniques [8]. Figures 2(c) and 2(d) show low-T $\rho(T)$ of $1T$-$Cu_{0.03}TiSe_2$ under pressures. The solid lines represent the fittings by the formula $\rho(T) = \rho_0 + AT^n$, where ρ_0 is the residual resistivity; the coefficient A and the temperature exponent n are related to the density of states at the Fermi

level and the inelastic electron scatterings, respectively [20]. Here, a polynomial fitting for T_c or $T^* < T < 20$ K gives ρ_0 and n, and a quadratic fitting for $n = 2$ to low temperature yields A. The pressure dependences of parameters ρ_0, A, and n are summarized in Figs. 3(b)–3(d). For S1# and S2#, with increasing pressure, ρ_0 decreases quickly with a slope change at P_c, and then shows a weak pressure dependence above P_c as shown in Fig. 3(b); the magnitude of the quadratic temperature coefficient A of normal-state resistivity enhances one order and reaches a maximum at P_c, which is positively correlated with the superconducting phase diagram under pressure. It is well known that the parameter A is proportional to the square of the Sommerfeld coefficient and reflects the density of states at the Fermi level $N(E_F)$ or the effective mass connected by $A \propto (m*/m_0)^2$ [29]. It is consistent with the increase of carrier concentration from CDW to SC by pressure and the enhanced CDW quantum fluctuations associated with the collapse of CDW, which supports the conclusions on unconventional SC [5,9]. Meanwhile, the n(AP) initially decreases from $\sim$3.31 at AP to a minimum $\sim$2.35 at P_c, and then increases slightly with pressure as indicated in Fig. 3(d). Such a reduction of the exponent n around P_c can be seen as evidence of enhanced CDW quantum fluctuations compared to the case of pure $1T$-$TiSe_2$ [5,13]. In addition, we can also note that low-temperature electrical resistivity under pressure deviates from the usual Fermi-liquid behavior ($n = 2$), and the evolution of the exponent indicates that the critical properties of the CDW phase are affected sensitively, such as electronic correlations and electron-phonon couplings, which are key factors for superconducting pairing. To sum up, our experimental results support the conclusions that the competition of CDW and SC as well as CDW critical fluctuation are critical factors for superconducting pairing.

Usually, the evolution of electronic structure under high pressure provides important information to deepen the understandings of phase diagrams. Figures 4(a)–4(c) show the field dependence of magnetoresistance (MR){= $[\rho_{xx}(H) - \rho_{xx}(0)]/\rho_{xx}(0)$} under pressures and temperatures for $1T$-$Cu_{0.03}TiSe_2$. At AP, the MR is plotted in Fig. 4(a) at various temperatures (5, 50, 100, 110, 120, 130, 150, and 200 K); the MR values at 5 and 50 K are found consistently and do not depend on the increasing ($0 \rightarrow 7$ T) and decreasing (7 T$\rightarrow 0$) processes; upon warming from low temperature and at AP, the MR (5 K, at 7 T) $\sim$0.73% decreases quickly to $\sim$0.14% at 100 K, and then reduces slightly to $\sim$0.07% at 200 K; upon increasing the pressure up to 1.50 GPa, the MR shows a similar temperature dependence, but its value (5 K, 7 T) enhances up to 2.61%, nearly 3.6 times larger than that at AP; meanwhile, the MR value (5 K, at 7 T) increases up to 6.09% at 3.0 GPa and then stays nearly constant until 7.0 GPa. The pressure and temperature dependence of MR just correspond to the collapse of the CDW: the MR values are sensitive to the pressure and temperature for $P < P_c$ and $T < T_{CDW}$ but tend to approach the saturated values once the CDW collapses.

Figures 4(d)–4(f) show the magnetic-field dependence of Hall resistivity $\rho_{xy}(H)$ under various pressures and temperatures for $1T$-$Cu_{0.03}TiSe_2$. At AP, $\rho_{xy}(H)$ remains negative, covering the whole temperature range (5–200 K), and its slopes $d\rho_{xy}(H)/dH$ change slightly with temperature.
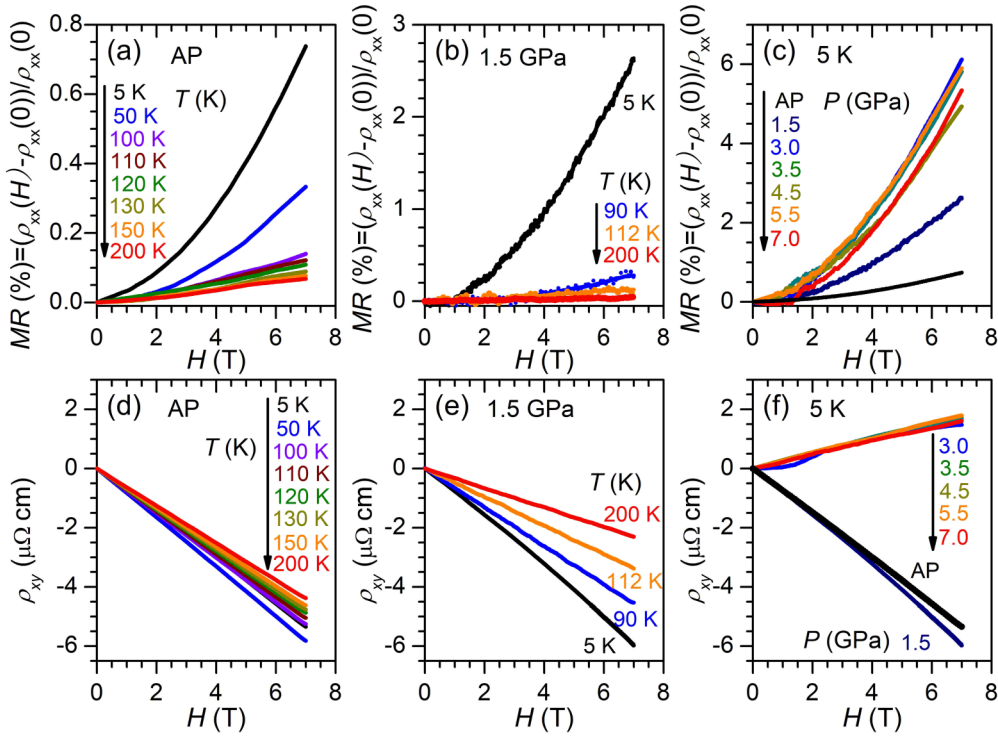
FIG. 4. Field dependence of transverse magnetoresistance MR $= [\rho_{xx}(H) - \rho_{xx}(0)]/\rho_{xx}(0)$ and longitudinal Hall resistivity $\rho_{xy}(H)$ at various temperatures and pressures: (a) MR at AP; (b) MR at 1.50 GPa; (c) MR at 5 K for various pressures; (d) $\rho_{xy}(H)$ at AP; (e) $\rho_{xy}(H)$ at 1.50 GPa; (f) $\rho_{xy}(H)$ at 5 K for various pressures; the black arrows indicate the changes of pressures and temperatures.

Meanwhile, upon increasing the pressure up to 1.50 GPa (lower than P_c), the sign of $\rho_{xy}(H)$ is still negative in 5–200 K, but its absolute value of $d\rho_{xy}(H)/dH$ decreases more obviously with the temperature than that at AP; above 3.0 GPa (higher than P_c), the sign of $\rho_{xy}(H)$ jumps to positive, which corresponds to the collapse of the long-range CDW. But $d\rho_{xy}(H)/dH$ barely changes in the pressure range of 3.0–7.0 GPa, which is consistent with the fact that electronic structures change slightly after the collapse of the CDW, and with the saturated tendency of the MR above P_c. Finally, these features of $1T$-Cu$_{0.03}$TiSe$_2$ suggest Fermi-surface reconstruction across CDW phase transition as in $1T$-TiSe$_2$ [6,7].

To clarify the evolution of the Fermi surface for $1T$-Cu$_{0.03}$TiSe$_2$, we conducted the Kohler analysis of the normalized MR and Hall conductivity under various temperatures and pressures in Fig. 5. As shown in Figs. 4(a)–4(c), the MR is an approximately quadratic field dependence at each temperature and pressure [30]. The normalized MR value versus $(\mu_0 H/\rho_0)^2$ was a linear dependence, and its slope changes sensitively as a function of temperature and pressure [7]. The fittings gave the Kohler slope K as evidence for the changes of Fermi surfaces [30]. The temperature dependence of K is compared for $1T$-Cu$_{0.03}$TiSe$_2$ and $1T$-TiSe$_2$ in Figs. 6(m)–6(o), and it will be discussed later. To specify the evolution of electronic structures, two-band analysis for the $\sigma_{xy}(H)$ was conducted as in Figs. 4(d)–4(f) and the fittings are in Figs. 5(d)–5(f): AP, 5–200 K in Fig. 5(d), 1.50 GPa; 5–200 K in Fig. 5(e); and 5 K, AP-7.0 GPa in Fig. 5(f), respectively. It is found that $\sigma_{xy}(H)$ has almost a linear dependence on magnetic field in the whole temperature range at AP and 1.50 GPa; up to 3.0 GPa, the sign of $\sigma_{xy}(H)$ changes suddenly from negative

to positive, which suggests the changes in type of the main carriers; more differently, $\sigma_{xy}(H)$ is nonlinear field dependence above 3.0 GPa, indicating some dramatic variations in electronic structure with the pressure-induced collapse of the CDW [7,14,31].

Based on two-band analysis of $\sigma_{xy}(H)$ [31,32], carrier concentrations (electron-type n_e, hole-type n_h, and the mobility of electrons μ_e and holes μ_h) were obtained; usually, the Hall conductivity with the two-band model is as follows:

$$\sigma_{xy} = \rho_{xy}/((\rho_{xy})^2 + (\rho_{xx})^2)$$
$$= \left(\frac{n_h \mu_h^2}{1 + (\mu_h B)^2} - \frac{n_e \mu_e^2}{1 + (\mu_e B)^2} \right) eB,$$

where n_e, μ_e and n_h, μ_h are the concentration and mobility of electron- and hole-type carriers, respectively. All the results are summarized in Figs. 6(a)–6(f). At AP, across the CDW phase transition, both n_e and n_h show a valley near the CDW phase transition; but the values of n_e are larger than n_h in the whole temperature range (5–300 K), which indicates that electron-type carriers are dominated; above T_{CDW}, n_e and n_h are close to each other, which is a feature of ordinary metal or semimetals. Such features are different from those in $1T$-TiSe$_2$ where electron-type carriers exceed hole-type carriers below T_{CDW} [6,7]. At 1.50 GPa similar behaviors are found, but both n_e and n_h have a larger temperature dependence than those at AP. In addition, the mobility of electrons and holes are almost equal for AP and 1.50 GPa; they both show slight decreases with increasing temperatures except for a jumpy increase at T_{CDW}. The decrease of mobility is attributed to the enhanced electron and phonon scattering at
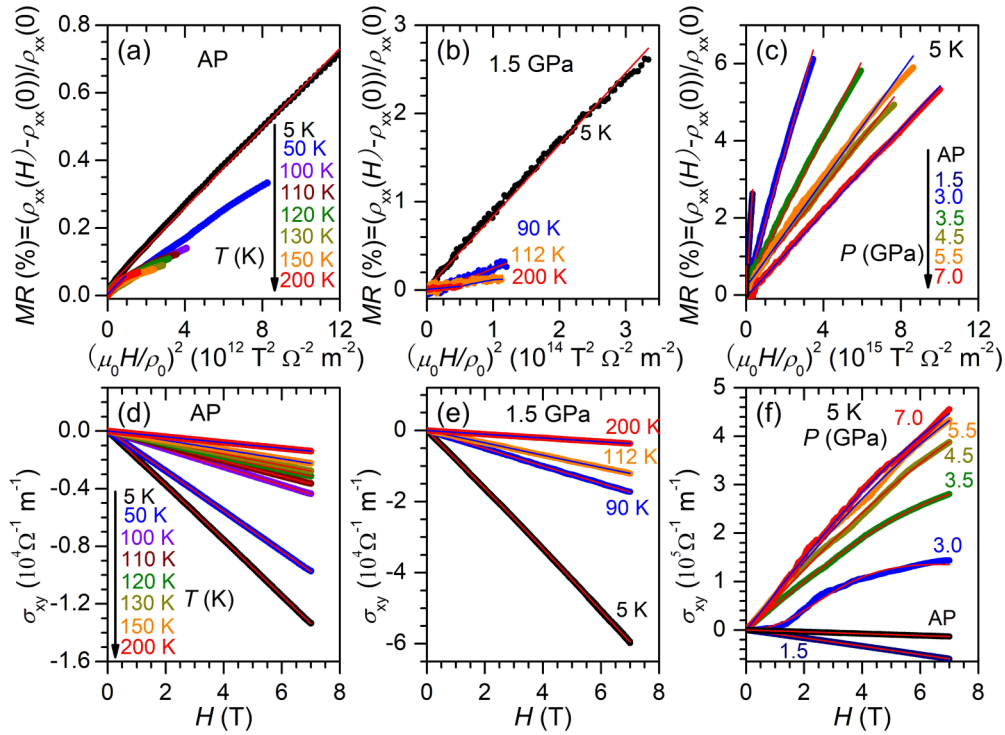
FIG. 5. The normalization of MR vs $(\mu_0 H/\rho_0)^2$ and linear fittings with Kohler slope; the MR and the linear fittings at various temperatures and pressures: (a) at AP for various temperatures; (b) at 1.50 GPa for various temperatures; (c) at 5 K for various pressures; solid lines indicate the fitting results; field dependence of Hall conductivity $\sigma_{xy}(H)$ and the fittings on the basis of two-band models: (d) $\sigma_{xy}(H)$ at AP; (e) $\sigma_{xy}(H)$ at 1.50 GPa; (f) $\sigma_{xy}(H)$ at 5 K; the black arrows indicate the changes of pressures and temperatures.

higher temperature, and the jumpy increase is attributed to the collapse of the CDW.

Along with the evolution of electronic structure, the MR is checked in Figs. 6(j) and 6(k). For AP and 1.50 GPa, the MR decreases on warming under various fields below T_{CDW} and keeps nearly constant values above T_{CDW}; in particular, it shows a jumpy increase near T_{CDW}, which is positively correlated with the increases of mobility. However, the enhancement in MR near T_{CDW} is gradually smoothed out under higher fields, which might be attributed to the reduced mobility. Upon further increasing the pressure up to 3.0 GPa, the n_h at 5 K increases quickly and surpasses n_e, and then it remains nearly constant until 7.0 GPa, which suggests that the dominant carrier changes from electron-type at AP to hole-type above P_c. In the same way, the mobility of electrons and holes is enhanced five times in magnitude near P_c as indicated in the derivative $d^2\rho/dP^2$ at 5 K. We can note that the enhancement of the mobility is larger than that as a function of temperature at AP and 1.5 GPa. At the same time, the MR shows a domelike pressure dependence at lower fields (0.5 T, 1.0 T), which is consistent with the enhancement of the mobility; when the fields are higher than 2.0 T, MR starts to increase with the pressure below P_c and trends to a saturated value above P_c. Besides, the Kohler slope K reduces quickly, as evidence of the variations of electronic structures such as the closing of the CDW gap. As shown in Fig. 6(m), the K value of $1T$-TiSe$_2$ increases upon warming below T_{CDW} and decreases quickly to nearly zero when the temperatures approach T_{CDW}. Thus, the decrease to nearly zero of the K can mark CDW phase transition [7,33]. For $1T$-Cu$_{0.03}$TiSe$_2$,

we note that K decreases with a smaller reduction compared to that of $1T$-TiSe$_2$, which is attributed to the partial closing of the CDW gap by Cu intercalation. Under pressure, the K reduces rapidly to nearly zero, which is consistent with the variation of T_{CDW}. These characteristics consistently indicate the high-pressure induced reconstruction of the Fermi surface in $1T$-Cu$_{0.03}$TiSe$_2$.

Finally, several important issues are discussed. The first one is the phase diagram of the CDW and SC in the Cu-underdoped $1T$-TiSe$_2$. As above, the double domelike T_c and T^* appear just after the collapse of CDW. The absent overlap of CDW and SC in pressure and composition phase diagrams clarifies that there should be strong competitions between them, and CDW fluctuations are critical for superconducting pairings; the evolution of characteristic parameters (ρ_0, A, n) of resistivity as a function of pressure supports our conclusions [5,20,27]. Meanwhile, the value of T_c^{onset} is highest just after the T^* disappears suddenly at 4.80 GPa, which can be seen as evidence of the possible competition of SC and some undetected orders associated with Kondo-like behavior. Similar to the case of $1T$-TiSe$_2$ [5], bulk SC and/or T_c^{zero} in $1T$-Cu$_{0.03}$TiSe$_2$ covers only a narrow pressure range, which is different from those of $1T$-TiSe$_2$ under pressure and the Cu intercalation [3,4] and electronic doping [13] at AP; the narrow Ti-3d electron bands and the absence of disorder scatterings under hydrostatic pressure are two possible reasons [25,34]. Secondly, it is unusual that the critical pressure of $1T$-Cu$_{0.03}$TiSe$_2$ ($P_c \sim 2.48$ GPa) is higher than that of $1T$-TiSe$_2$ ($P_c \sim 2$ GPa), although the Cu-intercalation can destroy the CDW effectively [5]. One possible reason
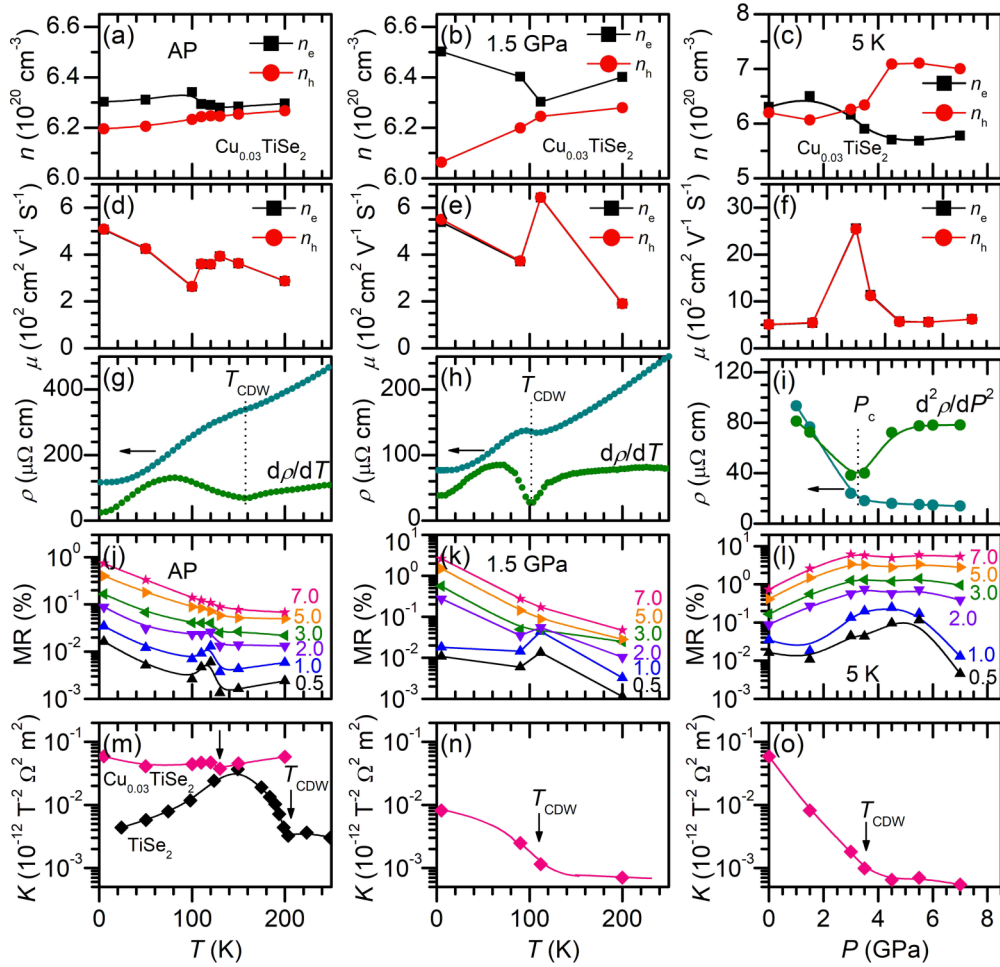
FIG. 6. Temperature dependence of carrier concentration, the electron-type n_e and the hole-type n_h at (a) AP and (b) 1.50 GPa; (c) n_e and n_h at 5 K, respectively; the mobility, μ_e and μ_h at (d) AP and (e) 1.50 GPa; (f) μ_e and μ_h at 5 K, respectively; $\rho(T)$ and $d\rho/dT$ at (g) AP and (h) 1.50 GPa; (i) $\rho(P)$ and $d^2\rho/dP^2$ at 5 K, respectively; MR at (j) AP and (k) 1.5 GPa under various fields; (l) pressure dependence of MR under various fields; Kohler slope K at (m) AP for $1T$-$Cu_{0.03}TiSe_2$ (pink) and $1T$-$TiSe_2$ (black) and (n) 1.50 GPa; (o) pressure dependence of K; the dashed lines and the arrows in (g),(h) and (m)–(o) indicate CDW phase transition; and the arrow in (i) indicates the P_c determined from the derivative $d^2\rho/dP^2$.

is the appearance of condensation of soliton dislocations of charges along with the injected charges by Cu-intercalation in $1T$-$TiSe_2$; meanwhile, it is well known that the slight Cu-intercalation could be inhomogeneous and randomly distributed in real space, which may induce weakly and strongly pinned regions under pressure; and the gradient of charges between them may be another factor affecting critical pressure. We believe that more in-depth research involving the mechanism of CDW is required.

Thirdly, $1T$-$TiSe_2$ undergoes Fermi surface reconstruction near T_{CDW} at AP with a clear change in type of main carriers, while the energy bands of $1T$-$Cu_{0.03}TiSe_2$ are dominated by electron-type carriers in the whole temperature range for $P < P_c$ and reverse into hole-type after the CDW collapse [7]. The distinct features indicate different electronic states of $1T$-$TiSe_2$ and $1T$-$Cu_{0.03}TiSe_2$ [3,5,10,18]. It is thought that an electron-type carrier is enhanced but a hole-type carrier reduces upon increasing the Cu intercalation in $1T$-$TiSe_2$, and then electron-pockets exceed hole-pockets in $1T$-$Cu_{0.03}TiSe_2$. Recent studies have revealed that both exciton pairings and electron-phonon couplings are necessary for the stability

of the CDW in $1T$-$TiSe_2$ [14]. Exciton pairing is partially destroyed because the Cu intercalation introduces electron doping and causes the decrease of CDW phase transition. The fourth one is the reason for the non-Fermi-liquid behavior near the critical pressure. As we know, the reduced crystal dimensionality and disorder scatterings typically limit the spatial range of nematic electronic order which usually originates from effective Fermi surface anisotropies/distortion due to the uniaxial anisotropy. In several unconventional SCs and strongly correlated electron materials such as iron-based high-T_c superconductors, the appearance of nematic phase usually causes non-Fermi-liquid behavior and strongly influences superconducting properties as well as the critical properties of the CDW; however, in $1T$-$TiSe_2$ and $1T$-Cu_xTiSe_2, no structural transition and/or broken rotational symmetry is involved in previous studies on TMDs in the literature, and there is no clear nematicity concerning CDW phase transitions.

The last one is the differences of superconducting properties via the Cu-intercalation and high pressure. The maximal $T_c^{max} \sim 4.15$ K for $1T$-Cu_xTiSe_2 ($x = 0.08$) is nearly two times larger than $T_c^{max} \sim 2.80$ K at 4.80 GPa in the

underdoped in $1T$-$Cu_{0.03}TiSe_2$ and the highest $T_c^{max} \sim$ 1.80 K in $1T$-$TiSe_2$ at 2.0–4.0 GPa; the difference is related to the distinct electronic state, i.e., the dominated electron-type carriers in $1T$-Cu_xTiSe_2 at AP are changed to hole-type ones in $1T$-$Cu_{0.03}TiSe_2$ at 4.80 GPa and $1T$-$TiSe_2$ at 2–4 GPa [3–5]; these features are contrary to the case of copper-based high-T_c superconductors where the maximal T_c of the electron-doping side is higher than that of the hole-doping side in the phase diagrams [35]. To clarify this issue, many interrelated factors including electronic correlations must be considered.

IV. CONCLUSION

We revisited the superconducting phase diagrams and electronic structures of the Cu-underdoped $1T$-$TiSe_2$ under hydrostatic pressure. It is found that the superconducting state just emerges after the collapse of the CDW; the super-conducting transition temperature shows a domelike pressure dependence with a maximum of $\sim$2.80 K at 4.80 GPa. Combined with the characteristic parameters, our present results consistently suggest the important role of the enhanced CDW fluctuation in gluing superconducting pairing; the evolution of carrier concentration, the mobility, and the Kohler slope are also studied by two-band analysis of Hall conductivity and the normalized magnetotransport. Energy bands are dominated by electron-type carriers below P_c and reverse into hole-type ones above P_c. Our results suggest the reconstruction of the Fermi surface along with the collapse of the CDW under pressure.

[1] M. Sarma, A. R. Beal, S. Nulsen, and R. H. Friend, J. Phys. C **15**, 4367 (1982).

[2] G. Grüner, Rev. Mod. Phys. **60**, 1129 (1988).

[3] E. Morosan, H. W. Zandbergen, B. S. Dennis, J. W. G. Bos, Y. Onose, T. Klimczuk, A. P. Ramirez, N. P. Ong, and R. J. Cava, Nat. Phys. **2**, 544 (2006).

[4] G. Wu, H. X. Yang, L. Zhao, X. G. Luo, T. Wu, G. Y. Wang, and X. H. Chen, Phys. Rev. B **76**, 024513 (2007).

[5] A. F. Kusmartseva, B. Sipos, H. Berger, L. Forro, and E. Tutis, Phys. Rev. Lett. **103**, 236401 (2009).

[6] A. Wegner, J. Zhao, J. Li, J. Yang, A. A. Anikin, G. Karapetrov, K. Esfarjani, D. Louca, and U. Chatterjee, Phys. Rev. B **101**, 195145 (2020).

[7] P. Knowles, B. Yang, T. Muramatsu, O. Moulding, J. Buhot, C. J. Sayers, E. Da Como, and S. Friedemann, Phys. Rev. Lett. **124**, 167602 (2020).

[8] Y. I. Joe, X. M. Chen, P. Ghaemi, K. D. Finkelstein, G. A. de la Pena, Y. Gan, J. C. T. Lee, S. Yuan, J. Geck, G. J. MacDougall, T. C. Chiang, S. L. Cooper, E. Fradkin, and P. Abbamonte, Nat. Phys. **10**, 421 (2014).

[9] A. Kogar, G. A. de la Pena, S. Lee, Y. Fang, S. X.-L. Sun, D. B. Lioi, G. Karapetrov, K. D. Finkelstein, J. P. C. Ruff, P. Abbamonte, and S. Rosenkranz, Phys. Rev. Lett. **118**, 027002 (2017).

[10] G. Li, W. Z. Hu, D. Qian, D. Hsieh, M. Z. Hasan, E. Morosan, R. J. Cava, and N. L. Wang, Phys. Rev. Lett. **99**, 027404 (2007).

[11] M. K. Wu, J. R. Ashburn, C. J. Torng, P. H. Hor, R. L. Meng, L. Gao, Z. J. Huang, Y. Q. Wang, and C. W. Chu, Phys. Rev. Lett. **58**, 908 (1987).

[12] F. Steglich, J. Aarts, C. D. Bredl, W. Lieke, D. Meschede, W. Franz, and H. Schäfer, Phys. Rev. Lett. **43**, 1892 (1979).

[13] L. Li, E. O'Farrell, K. Loh, G. Eda, B. Özyilmaz, and A. C. Neto, Nature (London) **529**, 185 (2015).

[14] M. Maschek, S. Rosenkranz, R. Hott, R. Heid, M. Merz, D. A. Zocco, A. H. Said, A. Alatas, G. Karapetrov, S. Zhu, J. van Wezel, and F. Weber, Phys. Rev. B **94**, 214507 (2016).

[15] S. Y. Li, G. Wu, X. H. Chen, and Louis Taillefer, Phys. Rev. Lett. **99**, 107001 (2007).

[16] J. Kačmarčík, Z. Pribulová, V. Paluchová, P. Szabó, P. Husaníková, G. Karapetrov, and P. Samuely, Phys. Rev. B **88**, 020507(R) (2013).

[17] D. Qian, D. Hsieh, L. Wray, E. Morosan, N. L. Wang, Y. Xia, R. J. Cava, and M. Z. Hasan, Phys. Rev. Lett. **98**, 117007 (2007).

[18] J. F. Zhao, H. W. Ou, G. Wu, B. P. Xie, Y. Zhang, D. W. Shen, J. Wei, L. X. Yang, J. K. Dong, M. Arita, H. Namatame, M. Taniguchi, X. H. Chen, and D. L. Feng, Phys. Rev. Lett. **99**, 146401 (2007).

[19] B. Sipos, A. Kusmartseva, A. Akrap, L. F. H. Berger, and E. Tutis, Nat. Mater. **7**, 960 (2008).

[20] B. S. Wang, Y. Liu, X. Luo, K. Ishigaki, K. Matsubayashi, W. J. Lu, Y. P. Sun, J.-G. Cheng, and Y. Uwatoko, Phys. Rev. B **97**, 220504(R) (2018).

[21] S. Kitou, A. Nakano, S. Kobayashi, K. Sugawara, N. Katayama, N. Maejima, A. Machida, T. Watanuki, K. Ichimura, S. Tanda, T. Nakamura, and H. Sawa, Phys. Rev. B **99**, 104109 (2019).

[22] N. Mori, H. Takahashi, and N. Takeshita, High Pressure Res. **24**, 225 (2004).

[23] J.-G. Cheng, K. Matsubayashi, S. Nagasaki, A. Hisada, T. Hirayama, M. Hedo, H. Kagi, and Y. Uwatoko, Rev. Sci. Instrum. **85**, 093907 (2014).

[24] See Supplemental Material at http://link.aps.org/supplemental/10.1103/PhysRevB.104.134503 for resistivity $\rho(T)$ for $1T$-$Cu_\delta TiSe_2$.

[25] K. Cho, M. Kończykowski, S. Teknowijoyo, M. A. Tanatar, J. Guss, P. B. Gartin, J. M. Wilde, A. Kreyssig, R. J. McQueeney,

A. I. Goldman, V. Mishra, P. J. Hirschfeld, and R. Prozorov, Nat. Commun. **9**, 2796 (2018).

[26] K. A. Gschneidner Jr, P. Burgardt, S. Legvold, J. O. Moorman, T. A. Vyrostek, and C. Stassis, J. Phys. F **6**, L49 (1976).

[27] B. S. Wang, Y. Liu, K. Ishigaki, K. Matsubayashi, J.-G. Cheng, W. J. Lu, Y. P. Sun, and Y. Uwatoko, Phys. Rev. B **95**, 220501(R) (2017).

[28] M. Monteverde, J. Lorenzana, P. Monceau, and M. Núñez-Regueiro, Phys. Rev. B **88**, 180504(R) (2013).

[29] J. Chen, L. Jiao, J. L. Zhang, Y. Chen, L. Yang, M. Nicklas, F. Steglich, and H. Q. Yuan, New J. Phys **15**, 053005 (2013).

[30] N. W. Ashcroft and N. D. Mermin, *Solid State Physics* (Saunders College, Philadelphia, 1976).

[31] Y. Ando, J. Phys. Soc. Jpn. **82**, 102001 (2013).

[32] A. Ikhwan, U. Saleheen, R. Chapai, L. Xing, R. Nepal, D. Gong, X. Gui, W. W. Xie, D. P. Young, E. W. Plummer, and R. Y. Jin, npj Quantum Mater. **5**, 53 (2020).

[33] M. K. Chan, M. J. Veit, C. J. Dorow, Y. Ge, Y. Li, W. Tabis, Y. Tang, X. Zhao, N. Barišić, and M. Greven, Phys. Rev. Lett. **113**, 177005 (2014).

[34] L. J. Li, X. Y. Deng, Z. Wang, Y. Liu, M. Abeykoon, E. Dooryhee, A. Tomic, Y. N. Huang, J. B. Warren, E. S. Bozin, S. J. L. Billinge, Y. P. Sun, Y. M. Zhu, G. Kotliar, and C. Perovis, npj Quantum Mater. **2**, 11 (2017).

[35] P. A. Lee, N. Nagaosa, and X.-G. Wen, Rev. Mod. Phys. **78**, 17 (2006).